

Development of G-P Zones on $\{111\}_{\text{Al}}$ Planes During Natural Aging of an Al-Zn-Mg-Cu-Zr Alloy

Ashim Kumar Mukhopadhyay and Konduri Satya Prasad

Defence Metallurgical Research Laboratory, Kanchanbagh, Hyderabad-500 058, India

The microstructure developed in an Al-Zn-Mg-Cu-Zr alloy with high Zn:Mg ratio following solution treatment and subsequent natural aging has been examined using a combination of conventional and high resolution transmission electron microscopic imaging and selected area electron diffraction methods. When naturally aged for 2 hours, the mottled microstructure contains a uniform and fine distribution of previously documented spherical Guinier-Preston (G-P) zones, as evidenced by selected area electron diffraction patterns (SAEDPs). No other second phase structure could be detected by SAEDPs in the alloy under this aging condition. In the case of the alloy naturally aged for 2 days, high resolution transmission electron microscopy (HRTEM) revealed a few 1 atom layer thick features lying on $\{111\}_{\text{Al}}$ crystallographic planes, in addition to the spherical G-P zones that dominated the microstructure. When naturally aged for 3 years, SAEDPs revealed characteristic diffraction spots due to spherical G-P zones (i.e. G-P I zones) as well as G-P II zones. The corresponding conventional transmission electron microscopic images distinctly revealed the presence of platelets lying on $\{111\}_{\text{Al}}$ planes. HRTEM revealed that the (i) plate shaped G-P zones nucleate independently in the matrix as well as on the $\{111\}_{\text{Al}}$ facets that develop upon the G-P I zones, and (ii) prolonged natural aging has the influence of typically producing 7 atom layer thick, fully coherent plate shaped G-P zones. The observation of characteristic diffraction spots due to G-P II zones from such plate shaped G-P zones point out that the G-P II zones nucleate and grow during natural aging.

Keywords: Al-Zn-Mg-Cu-Zr alloy; natural aging; transmission electron microscopy; plate shaped G-P zones

1. Introduction

In the nucleation of precipitates from solid solution, the formation of various transition phases and equilibrium phases occurs in order of increasing precipitate: matrix interfacial energy [1, 2]. Consequently, upon solution treatment, the decomposition of supersaturated solid solution in most precipitation hardening aluminium alloys begins with the formation of fully coherent Guinier-Preston (G-P) zones. In Al-Zn-Mg alloys, the precipitation reactions occurring in the sequence of G-P zones $\rightarrow \eta' \rightarrow \eta$ (MgZn_2) & T [$(\text{AlZn})_{49}\text{Mg}_{32}$], the first phase precipitate to form during or immediately after quenching is the spherical G-P zones. The spherical G-P zones contain both Zn & Mg, and such zones nucleate and grow during natural aging [3, 4]. In Cu-bearing Al-Zn-Mg alloys too, the spherical G-P zones are the first to form during or immediately after quenching and the G-P zones nucleate and grow during natural aging [5]. The spherical G-P zones (termed G-P I zones) are ordered as originally proposed by Schmalzried and Gerold [6]. Recent studies using atom probe field ion microscopy (APFIM) [7] and HRTEM [8], however, failed to detect ordering in such G-P zones. In Al-Zn-Mg base alloys, the spherical G-P zones give rise to diffuse electron diffraction spots near the forbidden $\{100\}_{\text{Al}}$ and around the forbidden $\{110\}_{\text{Al}}$ positions in $\langle 100 \rangle_{\text{Al}}$ projections [9].

In recent years, several workers using *artificially aged* Al-Zn-Mg alloys have demonstrated that there exists a second type of G-P zones, termed G-P II [8-12]. G-P II zones have been described as "thin objects parallel to $\{111\}_{\text{Al}}$ planes", 1-2 atom layer thick and 3-6 nm wide [8]. The G-P II zones are understood to be Zn-rich clusters representing the G-P zones in the constituent Al-Zn system in ternary Al-Zn-Mg alloys: the G-P zones in the binary Al-Zn system produce electron diffraction effects that are identical to those due to the G-P II zones in the Al-Zn-Mg system [10]. Characteristic

diffuse electron diffraction spots due to G-P II zones appear near $\frac{2}{3}\{220\}_{\text{Al}}$ positions in $\langle 001 \rangle_{\text{Al}}$ projections [9], slightly outside $\frac{1}{3}\{422\}_{\text{Al}}$ positions in $\langle 111 \rangle_{\text{Al}}$ projections [8] and near $\frac{1}{2}\{311\}_{\text{Al}}$ positions in $\langle 112 \rangle_{\text{Al}}$ projections [8].

However, there are conflicting reports regarding the nucleation, growth, stability and morphology of G-P II zones in the literature e.g. (1) there exists no observable difference between G-P I and G-P II; both types of precipitates, when examined by APFIM, appeared spherical [9], (2) G-P II zones form during quenching, but they do not grow during natural aging [12], (3) growth of G-P II zones occur at temperatures above 70°C [8, 11, 12], (4) Cu addition retards the formation of G-P II zones at room temperature [13] and (5) G-P II zones are not observed in commercial alloy AA7050 during any stage of aging at 121°C [14]. It is the purpose of the present investigation to study the formation and growth of plate shaped G-P II zones during natural aging of an Al-Zn-Mg-Cu-Zr alloy. The importance of this study is significant because, the G-P II zones are understood to play a major role in the nucleation of the strengthening η' plates during subsequent artificial aging of 7xxx series Al alloys.

2. Experimental Procedure

The aluminium alloy used in the present investigation has the composition (wt%) of Al-11.8Zn-1.5Mg-1.7Cu-0.16Zr-0.12Fe-0.08Si. Fe and Si impurities were associated with the primary aluminium that was used to prepare the alloy. The Zn content of the alloy was maintained rather high, because Zn is understood to be the major alloying element influencing the formation of “Zn-rich” G-P II zones during quenching and/or subsequent natural aging or early stages of artificial aging. Whilst, the Cu and Mg were kept at relatively moderate levels in order for the alloy to get substantially homogenized using the commercially viable homogenization treatment. The slightly higher Zr content of 0.16% was utilized in the alloy in order to keep the percentage recrystallization to a minimum in the fully heat treated wrought products.

The alloy was prepared in an induction furnace under argon atmosphere. The resultant as-cast billet (\varnothing 75 mm) was homogenized, scalped and hot deformed to 18 mm diameter round bar extrusions. The extrusions were solution treated at 455°C for 1.5 h. The quenching from the solution treatment temperature was carried out in water at ambient temperature. The extrusions were then naturally aged for a period up to 3 years. Tensile tests carried out on the alloy samples naturally aged for 3 years revealed an average 0.2% PS of 685 MPa, thereby indicating a very substantial increase in the strength of the alloy during natural aging. Tensile testing was carried out at ambient temperature on round tensile specimens (25 mm gauge length) using INSTRON 8500 testing machine at a cross-head speed of 1.0 mm min⁻¹.

A combination of TEM and HRTEM was carried out to characterize the microstructure developed during natural aging of the alloy. TEM was carried out on a FEI TECNAI 20T electron microscope operating at 200 kV. HRTEM was carried out on a TECNAI 20 UT high resolution transmission electron microscope operating at 200 kV.

3. Results and Discussion

Figure 1(a) represents a transmission electron micrograph (in $\langle 001 \rangle_{\text{Al}}$ projection) from the alloy naturally aged for 2 h. The micrograph shows the presence of a non-uniform distribution of spherical, ordered ($L1_2$) Al_3Zr dispersoids, as evidenced by the

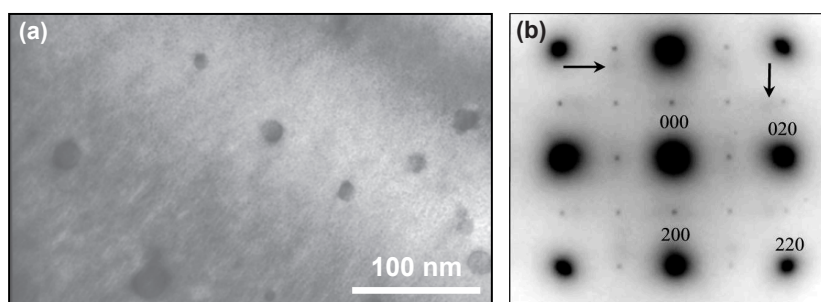


Fig. 1. (a) Transmission electron micrograph (in $\langle 001 \rangle_{\text{Al}}$ projection) obtained from the alloy naturally aged for 2 h. (b) The corresponding SAEDP showing diffuse diffraction spots (a couple marked by arrows) due to G-P I zones.

superlattice reflections present in the corresponding SAEDP shown in Figure 1(b). The micrograph further shows the presence of a uniform and fine distribution of spherical G-P zones, as evidenced by the characteristic diffuse diffraction spots near the forbidden $\{100\}_{\text{Al}}$ positions [a couple of spots marked by arrows in Figure 1(b)].

Figure 2 represents a high resolution transmission electron micrograph (in $\langle 011 \rangle_{\text{Al}}$ projection) from the alloy naturally aged for 2 days. The micrograph shows the presence of a 1 atom layer thick feature (marked by arrows) exhibiting dark contrast compared to the surrounding matrix. Associated strain field present on one side of the feature may further be noted. Fast Fourier transform (FFT) of such features always produced streaks in the direction normal to its habit plane i.e. $\{111\}_{\text{Al}}$ planes (see the inset in Figure 2).

Figure 3(a) represents a transmission electron micrograph (in $\langle 011 \rangle_{\text{Al}}$ projection) obtained from the alloy naturally aged for 3 years. The most significant feature of the micrograph is the presence of thin platelets along $\{111\}_{\text{Al}}$ planes (a few marked by arrows). Figure 3(b) represents the SAEDP obtained from Figure 3(a). The superlattice reflections due to the Al_3Zr dispersoids may be noted in the SAEDP. The faint streaks along $\langle 111 \rangle_{\text{Al}}$ directions due to the thin platelets on $\{111\}_{\text{Al}}$ planes are further noteworthy. Yet another noteworthy feature is the presence of diffraction spots at $\frac{1}{3}\{220\}_{\text{Al}}$ and $\frac{2}{3}\{220\}_{\text{Al}}$ positions (one set of spots marked by arrows) that have been known to be due only to the η' precipitates [15]. It may be noted that faint and diffuse diffraction spots at $\frac{1}{3}\{220\}_{\text{Al}}$ and $\frac{2}{3}\{220\}_{\text{Al}}$ positions are as well present in the SAEDPs obtained in $\langle 001 \rangle_{\text{Al}}$ and $\langle 112 \rangle_{\text{Al}}$ projections, as shown in Figures 3(c) and 3(d), respectively. The diffuse diffraction spots due to the G-P I zones may be noted in Figure 3(c). In $\langle 112 \rangle_{\text{Al}}$ projections, the presence of diffraction spots near $\frac{1}{2}\{311\}_{\text{Al}}$ positions due to G-P II zones [8] may further be noted. Figure 3(e) represents a transmission electron micrograph obtained from a different region of the same thin foil in a 2-beam condition ($g_{\bar{1}\bar{1}\bar{1}}$) near $\langle 011 \rangle_{\text{Al}}$ projection. The micrograph distinctly shows the presence of plate shaped precipitates (a couple marked by arrows) under this aging condition.

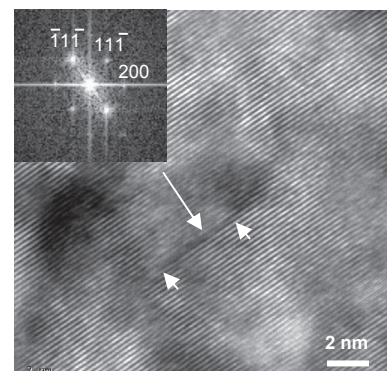


Fig. 2. High resolution transmission electron micrograph (in $\langle 011 \rangle_{\text{Al}}$ projection) showing a 1 atom layer thick feature (marked by arrows) lying on $\{111\}_{\text{Al}}$ planes. The inset represents a fast Fourier transform of the feature.

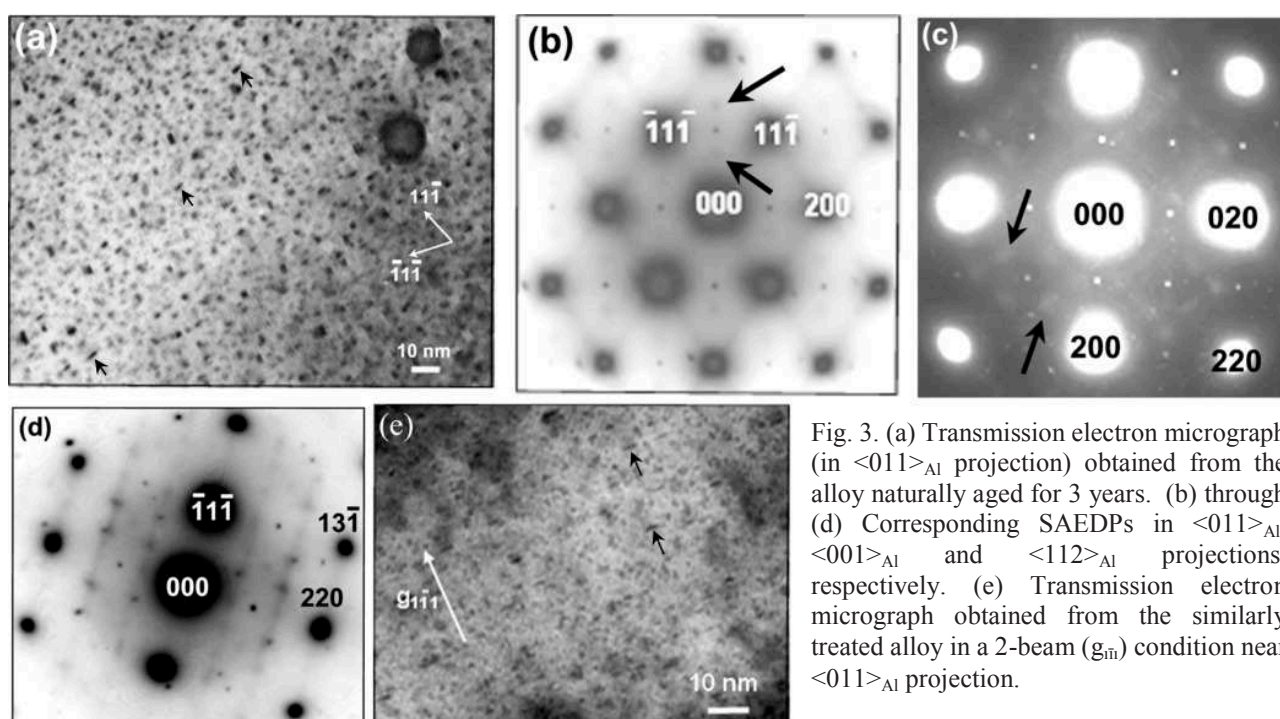


Fig. 3. (a) Transmission electron micrograph (in $\langle 011 \rangle_{\text{Al}}$ projection) obtained from the alloy naturally aged for 3 years. (b) through (d) Corresponding SAEDPs in $\langle 011 \rangle_{\text{Al}}$, $\langle 001 \rangle_{\text{Al}}$ and $\langle 112 \rangle_{\text{Al}}$ projections, respectively. (e) Transmission electron micrograph obtained from the similarly treated alloy in a 2-beam ($g_{\bar{1}\bar{1}\bar{1}}$) condition near $\langle 011 \rangle_{\text{Al}}$ projection.

Figure 4(a) represents a centred dark field (CDF) image using $\frac{2}{3}\{220\}_{Al}$ reflections from G-P II zones in $\langle 001 \rangle_{Al}$ projection of the alloy naturally aged for 3 years. The plate shape of the G-P II zones is evident. Figures 4(b) & (c) represent CDF images using $\frac{2}{3}\{220\}_{Al}$ and $\frac{1}{2}\{113\}_{Al}$ reflections, respectively due to the plate shaped G-P II zones in $\langle 112 \rangle_{Al}$ projections in a different region of the same thin foil. Figure 4(d) represents an SAEDP in $\langle 111 \rangle_{Al}$ projection, and Figure 4(e) represents a CDF image using reflections near $\frac{2}{3}\{422\}_{Al}$ due to G-P II zones.

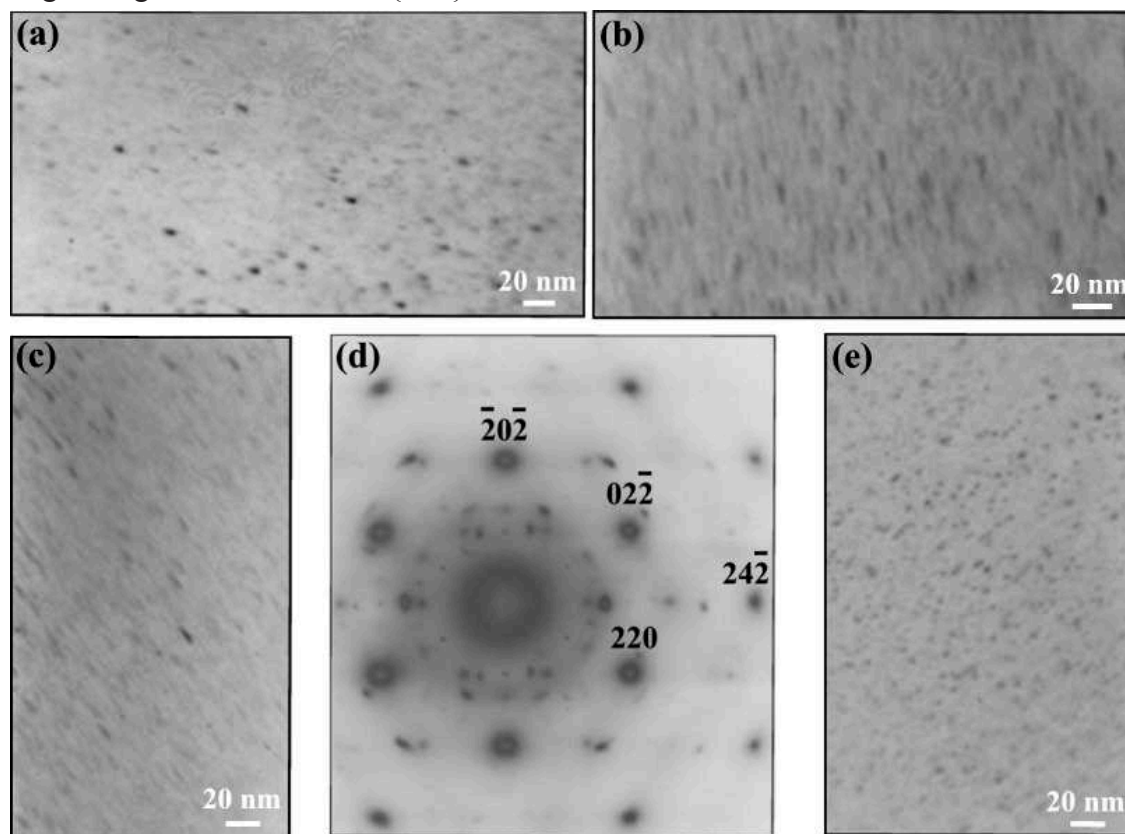


Fig. 4. Centred dark field images using (a) $\frac{2}{3}\{220\}_{Al}$ reflections due to G-P II zones in $\langle 001 \rangle_{Al}$ projection, and (b) $\frac{2}{3}\{220\}_{Al}$ reflections, & (c) $\frac{1}{2}\{113\}_{Al}$ reflections due to G-P II zones in $\langle 112 \rangle_{Al}$ projections. (d) SAEDP in $\langle 111 \rangle_{Al}$ projection, and (e) CDF image using G-P II reflections near $\frac{2}{3}\{422\}_{Al}$ in $\langle 111 \rangle_{Al}$ projection.

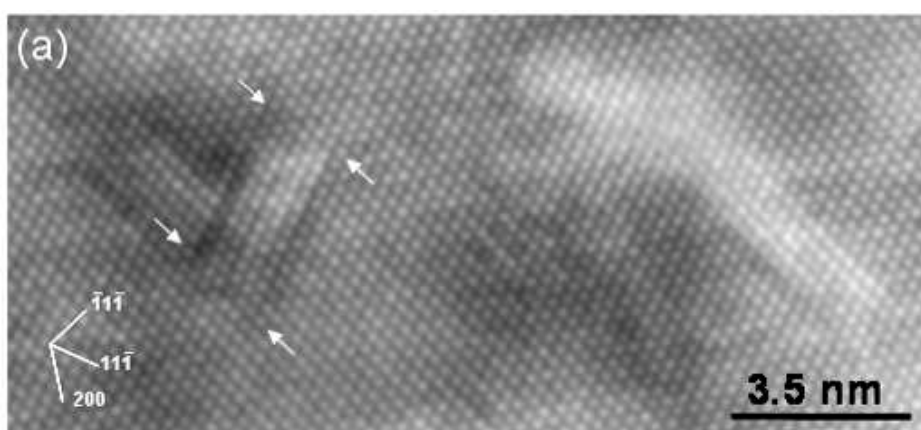


Figure 5(a) represents an HRTEM image (in $\langle 011 \rangle_{Al}$ projection) showing the presence of fully coherent plate shaped G-P zones developed during natural aging. Close examination of the micrograph reveals that in all cases, typically 5 atom layers of relatively

bright contrast followed by one more 1 atom layer of dark contrast had grown on to the 1 atom layer features that formed first on $\{111\}_{Al}$ planes early during the natural aging cycle. The dark contrast of the two 1 atom layers (each such layer of a plate shaped G-P zone marked by small arrows) compared to the relatively less darker to bright contrast of the 5 atom layers tend to imply that the initial 1 atom layer must be rich in Zn atoms, whilst the subsequent 5 atom layers must involve further elemental atoms having lower atomic number such as Mg [3]. This is because Zn has higher atomic

scattering amplitude for electrons than Mg has [16]. Like Zn, Cu also has higher atomic scattering amplitude for electrons, however, Cu usually has the tendency to segregate on $\{100\}_{\text{Al}}$ planes rather than on $\{111\}_{\text{Al}}$ planes [17].

Figure 5(b) represents an HRTEM image (in $\langle 011 \rangle_{\text{Al}}$ projection) obtained from a different region of the same thin foil. The presence of several fully coherent, plate shaped G-P zones is noteworthy. The insets i.e. the fast Fourier transform of the plate shaped G-P zones showing streaks in the directions normal to the habit plane of the G-P zones (due to the shape factor) may further be noted. The dimensions of these G-P zones are comparable with those observed in Figure 3.

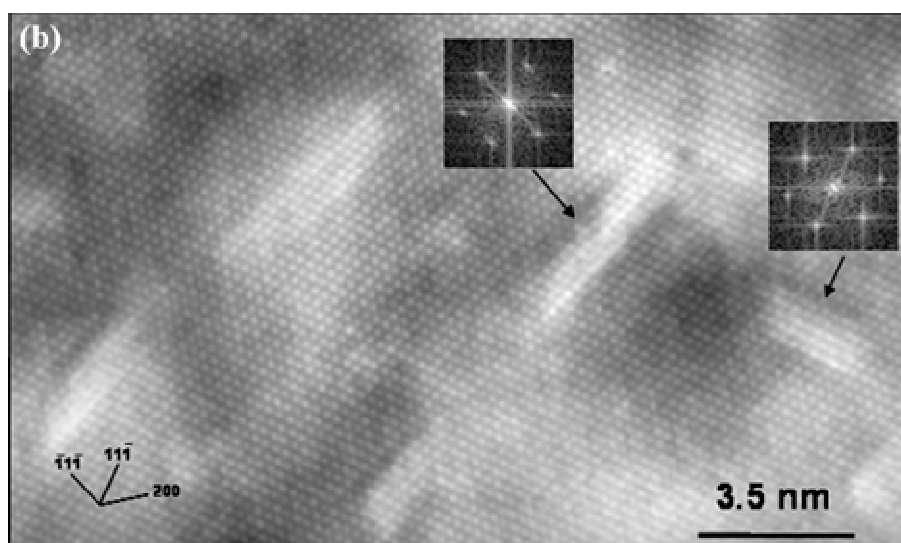


Fig. 5. (a) & (b) High resolution transmission electron micrographs (in $\langle 011 \rangle_{\text{Al}}$ projections) obtained from the alloy naturally aged for 3 years showing the formation of plate shaped G-P zones. The fast Fourier transform (FFT) of such zones containing the 1 atom layer features of dark contrast always showed streaks (see the insets) in the directions normal to the habit planes of such plate shaped G-P zones.

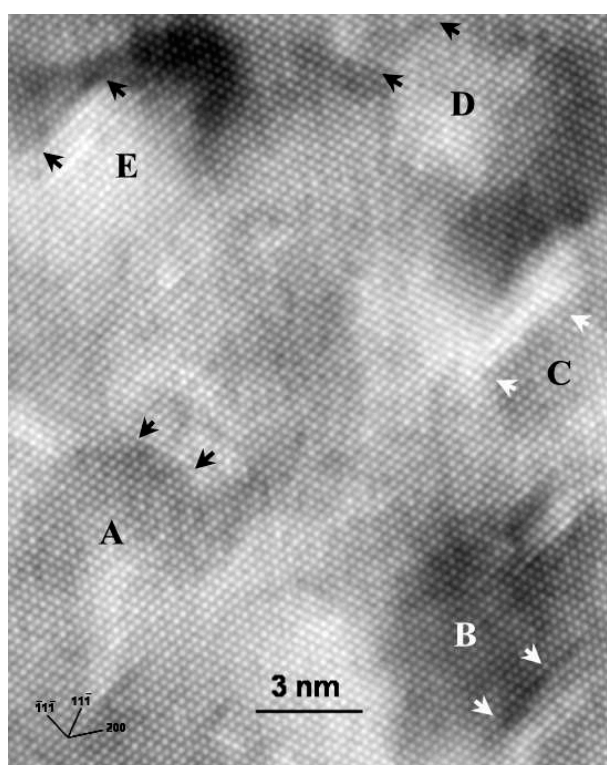


Fig. 6. High resolution transmission electron micrograph (in $\langle 011 \rangle_{\text{Al}}$ projection) obtained from the alloy naturally aged for 3 years showing formation of faceted G-P I zones (labelled A-E), and nucleation of G-P II zones (marked by arrows) upon the $\{111\}_{\text{Al}}$ facets developed on the G-P I zones.

The formation of typically a total of 7 atom layers in the plate shaped G-P zones tends to account for the $6 \times d_{\{111\}_{\text{Al}}} = 1.40$ nm i.e. one of the lattice parameters of the hexagonal η' precipitates (i.e. $a = 0.496$ nm and $c = 1.40$ nm) [15] that will have formed during artificial aging at appropriate aging temperatures following the requisite compositional and crystal structural changes within such G-P zones. The fully coherent, plate shaped precipitates developed during natural aging of the present alloy must, therefore, represent the G-P II zones that were previously documented only in the *artificially aged* Al-Zn-Mg alloys of varying compositions [8-12]. The present results and interpretations, on the other hand, provide definite information regarding the very early stages of formation of G-P II zones and throw light on the ways how such G-P zones could serve as the basis for the formation of η' plates during artificial aging.

Figure 6 represents an HRTEM image showing several faceted G-P I zones (labeled A through E). The presence of 1 atom layer thick features of dark contrast (marked by arrows) on the $\{111\}_{\text{Al}}$ facets developed on the G-P I zones may be noted. In many cases, further atom layers grew onto the 1 atom layer thick features, as discussed earlier in this communication. Firstly, the formation of

faceted G-P zones parallels the previously documented results on the formation of faceted G-P zones during the early stages of artificial aging (i.e. 1.5 h at 100°C) of an Al-5Zn-2Mg (wt %) alloy [18]. Secondly, the nucleation of one phase at the interface boundaries of the predecessor phase is rather a proven phenomenon in the solid state nucleation reactions in age hardening Al alloys [1, 2]. In the present case, such a phenomena is facilitated because both the crystallographic planes of the facets and the habit planes of the G-P II zones is $\{111\}_{Al}$. The present study, therefore, establishes that the nucleation of fully coherent G-P II zones occurs independently in the matrix as well as upon the $\{111\}_{Al}$ facets developed on the G-P I zones.

4. Summary and Conclusions

In a wrought Al-Zn-Mg-Cu-Zr alloy containing 11.8 wt% Zn, the formation of plate shaped G-P zones occurs during natural aging. The fully coherent, plate shaped G-P zones, nucleate on $\{111\}_{Al}$ planes independently in the matrix as well as upon the $\{111\}_{Al}$ facets developed on the G-P I zones. Initially, such G-P zones are 1 atom layer thick, and the fast Fourier transform (FFT) of such features always gives rise to streaks in the direction normal to its habit planes. Prolonged natural aging has the effect of forming a total of 7 atom layers in the plate shaped G-P zones. Such plate shaped G-P zones could be viewed in CDF images using characteristic reflections known to be due to the G-P II zones implying that the G-P II zones nucleate and grow during natural aging.

Acknowledgement

The authors wish to acknowledge the financial support of Defence Research and Development Organization (DRDO), Government of India.

References

- [1] E. Hornbogen: *Z. Metallk.* 56 (1965) 133-154.
- [2] K. C. Russell and H.I.Aaronson: *J. Mater. Sci.* 10 (1975) 1991-1999.
- [3] A. K. Mukhopadhyay: *Phil. Mag. Lett.*, 70 (1994) 135-140.
- [4] A. K. Mukhopadhyay, Q. B. Yang, S. R. Singh: *Acta Metall.* 42(9) (1994) 3083-3091.
- [5] A.K.Mukhopadhyay: *Trans. IIM*, 2(2) (2009) 113-122.
- [6] H. Schmalzried and V. Gerold: *Z. Metallk.*: 49 (1959) 291-301.
- [7] S. K. Maloney, K. Hono, I. J. Polmear and S. P. Ringer: *Scripta Mater.* 41(10) (1999) 1031-1038.
- [8] L. K. Berg, J. Gjønnes, V. Hansen , X. Z. Li, M. Knutson-Wedel, G. Waterloo, D. Schryvers and L. R. Wallenberg, *Acta Mater.*, 49 (2001) 3443-3451.
- [9] K. Stiller, P.J. Warren, V. Hansen, J. Angenete and J. Gjønnes: *Mater. Sci. Engg.* A270 (1999) 55-63.
- [10] X. J. Jiang, B. Noble, B. Holme, G. Waterloo and J. Tafto: *Metall. Mater. Trans. A.* 31A (2000) 339-348.
- [11] V. Hansen, O. B. Karlsen, Y. Langsrud and J. Gjønnes: *Mater. Sci. Technol.* 20 (2004) 185-193.
- [12] A. Dupasquier, R. Ferragut, M. M. Iglesias, M. Massazza, G. Riontino, P. Mengucci, G. Barucca, C. E. Macchi and A. Somoza: *Phil. Mag.* 87 (2007) 3297-3323.
- [13] X. J. Jiang, B. Noble, V. Hansen and J. Tafto: *Metall. Mater. Trans. A.* 32A (2001) 1063-1073.
- [14] G. Sha and A. Cerezo: *Acta Mater.* 52 (2004) 4503-4510.
- [15] J. K. Park and A. J. Ardell: *Metall. Mater. Trans. A.* 14A (1983) 1957-1965.
- [16] P. B. Hirsch, A. Howie, R. B. Nicholson, D. W. Pashley and M. J. Whelan: *Electron Microscopy of Thin Crystals* (Malabar, Florida: R. E. Krieger, 1977) pp. 505.
- [17] A. Kelly and R. B. Nicholson: *Prog. in Mat. Sci.* 10 (1963) 148-391.
- [18] C. E. Lyman and J. B. Vander Sande: *Metall. Trans.* 7A (1976) 1211-1216.